

The PANS k – ε model in a zonal hybrid RANS–LES formulation



L. Davidson*

Division of Fluid Dynamics, Department of Applied Mechanics, Chalmers University of Technology, SE-412 96 Gothenburg, Sweden

ARTICLE INFO

Article history:

Received 2 July 2013

Received in revised form 22 November 2013

Accepted 7 January 2014

Keywords:

LES

PANS

2G-RANS

Zonal model

Embedded LES

Hybrid RANS–LES

ABSTRACT

A new approach to use the partially averaged Navier–Stokes (PANS) model as a hybrid RANS–LES model is presented. It is evaluated in fully developed channel flow and embedded LES in a hump flow. For the channel flow, the two RANS–LES interfaces are parallel to the walls. In the URANS region, f_k is set to one. In the LES region, f_k is set to a constant value (the baseline value is $f_k = 0.4$) or it is computed. It is found that the new model gives good results for channel flow for a large span of Reynolds numbers ($4000 \leq Re_\tau \leq 32,000$). In the channel flow simulations, three different grids are used in the wall-parallel planes, 32^2 , 64^2 and 128^2 , and the model yields virtually grid-independent flow fields and turbulent viscosities. Embedded LES is used for the hump flow which is well predicted. The RANS–LES interface is normal to the flow from the inlet. RANS is used upstream of the interface. Downstream this interface, RANS is used near the wall and LES is used away from the wall.

© 2014 Elsevier Inc. All rights reserved.

1. Introduction

Wall-bounded Large Eddy Simulation (LES) is affordable only at low Reynolds number. At high Reynolds number, the LES must be combined with a URANS treatment of the near-wall flow region. There are different methods for bridging this problem such as Detached Eddy Simulation (DES) (Spalart et al., 1997; Spalart, 2000; Shur et al., 2008), hybrid LES/RANS (Davidson and Peng, 2003; Temmerman et al., 2005) and Scale-Adapted Simulations (SAS) (Menter and Egorov, 2010; Egorov et al., 2010); for a review, see Fröhlich and von Terzi (2008). The two first classes of models take the SGS length scale from the cell size whereas the last (SAS) involves the von Kármán lengthscale.

The DES, hybrid LES/RANS and the SAS models have one thing in common: in the LES region, the turbulent viscosity is reduced. This is achieved in different ways. In some models, the turbulent viscosity is reduced indirectly by increasing the dissipation term in the k equation as in two-equation DES (Travin et al., 2000). In other models, such as in the two-equation X-LES (Kok et al., 2004) and in the one-equation hybrid LES–RANS (Davidson and Billson, 2006; Temmerman et al., 2005), it is accomplished by reducing the length scale in both the expression for the turbulent viscosity as well as for the dissipation term in the k equation.

In the partially averaged Navier–Stokes (PANS) model (Girimaji, 2006a) and the Partially Integrated Transport Model (PITM) (Schiestel and Dejoan, 2005; Chaouat and Schiestel, 2005), the turbulent viscosity is reduced by decreasing the destruction term

in the dissipation (ε) equation which increases ε . This decreases the turbulent viscosity in two ways: first, the turbulent viscosity is reduced because of the enhancement of ε , and, second, the turbulent kinetic energy, k , decreases because of the increased dissipation term, ε .

In the SAS model based on the k – ω model, the turbulent viscosity is reduced by an additional source term, P_{SAS} , in the ω equation. The source term is activated by resolved turbulence; in steady flow it is inactive. When the momentum equations are in turbulence-resolving mode, P_{SAS} increases which increases ω . This decreases the turbulent viscosity in two ways: first, directly, because ω appears in the denominator in the expression for the turbulent viscosity, ν_t , and, second, because k is reduced due to its increased dissipation term $\beta^* k \omega$.

The PANS model and the PITM models are very similar to each other although their derivations are completely different. The only difference in the models is that in the PANS model the turbulent diffusion coefficients in the k and ε equations are modified. These two models do not use the filter width, and can hence be classified as URANS models. On the other hand, a large part of the turbulence spectrum is usually resolved which is in contrast to standard URANS models. PANS and PITM models have by Fröhlich and von Terzi (2008) been classified as second-generation URANS models, or 2G-URANS models.

The PANS model is used in the present work. In PANS, two new coefficients are introduced, f_k and f_ε . The former denotes the ratio of the modeled to the total turbulent kinetic energy, and the latter denotes the corresponding ratio of the dissipation. Since small turbulent scales affected by dissipation are not resolved in the present study, the coefficient f_ε is set to one. The coefficient f_k may vary

* Tel.: +46 31 7221404.

E-mail address: lada@chalmers.se

from one (RANS) to zero (DNS). For LES it should take values somewhere in between. When using PANS in turbulence-resolving mode, f_k is usually set to a constant value (both in space and time). In [Girimaji \(2006b\)](#) they used a constant f_k , mostly 0.4 and 0.5. [Frendia et al. \(2006\)](#) used a constant f_k coefficient of 0.2 and set $f_\varepsilon = 0.5$, 0.667 or 1.0. They found that $f_\varepsilon = 0.667$, i.e. $f_k/f_\varepsilon = 0.3$, gave the best results on the chosen grid. In [Ji et al. \(2011, 2012\)](#) they used constant values of f_k for simulating cavitating flow around an hydrofoil and a cavitating propeller. They found that the smaller f_k , the higher the shedding frequency. They recommend a value of $f_k = 0.2$. In [Girimaji and Abdol-Hamid \(2005\)](#) they used either a constant f_k in space (in the range $0.4 < f_k < 1$) or they let f_k vary. They compute it as $3(\Delta_{\min}/L_t)^{2/3}$ where Δ_{\min} is the smallest grid cell size and $L_t = (k + k_{\text{res}})^{3/2}/\varepsilon$ where $k + k_{\text{res}}$ denotes modeled plus resolved turbulent kinetic energy. They obtained the space-varying f_k from a pre-cursor steady RANS simulation and then kept it constant in time in the PANS simulations. The lowest constant value, $f_k = 0.4$, gave the best results. [Lakshmipathy et al. \(2011\)](#) used PANS for vortex shedding around a circular cylinder at high Reynolds number. The evaluated different constant f_k values (0.5, 0.6, 0.7, 1.0) and they found that $f_k = 0.5$ gave best agreement with experiments. [Basu et al. \(2007\)](#) propose a new form of varying f_k . They present results also for constant f_k using 0.3, 0.75 and 0.85. They show that the varying f_k and $f_k = 0.3$ give good results. Furthermore, it is shown that when the varying f_k method is used, f_k takes values between 0.2 and 0.4 in the turbulence-resolving regions. An extension of PANS, based on a four-equation k – ε – ζ – f model, was recently proposed ([Basara et al., 2011](#)). They compute f_k as $C_\mu^{-1/2}(\Delta/L_t)^{2/3}$ where $\Delta = V^{1/3}$ (V denotes cell volume). A near-wall low-Reynolds number capability was added to PANS so that the equations can be integrated all the way up to the wall ([Ma et al., 2011](#)). In that work, it was furthermore shown that the PANS model is a good SGS model for wall-resolved LES at low Reynolds numbers. It was found that a constant value of $f_k = 0.4$ was appropriate. [Davidson and Peng \(2011, 2013\)](#) present embedded LES applied to channel flow and the flow over a hump. [Davidson \(2012\)](#) used PANS in LES mode of a developing boundary layer and the flow over a backstep. Different constant f_k values were evaluated in these works. A value of $f_k = 0.4$ was recommended.

In the present work, the PANS model is used as a zonal hybrid LES/RANS model to simulate wall-bounded flow at high Reynolds number. $f_k = 1$ in the near-wall region, and $f_k < 1$ in the LES region. Different constant values of f_k have been used in the literature, see above. A value of $0.4 \leq f_k \leq 0.5$ has been shown to be best in most of the works, except in cavitating flow where a value of 0.2 was found to be optimal. Based on the work in the literature, a baseline value of $f_k = 0.4$ is chosen for the LES region in the present work. Constant f_k values in the range $0.2 \leq f_k \leq 0.6$ are also evaluated. Although most investigations in the literature have used a constant f_k , it should conceptionally be dependent on the grid size. A smaller f_k should be used when the grid is refined and vice versa. Hence, simulations are also carried out in the present study using a variable f_k in space where $f_k = C_\mu^{-1/2}(\Delta/L_t)^{2/3}$ as proposed by [Basara et al. \(2011\)](#).

The paper is organized as follows: the equations and the modeling are presented in the next section followed by a description of the numerical method. The following section presents and discusses the results and conclusions are drawn at the end of the paper.

2. Equations

2.1. Mean flow equations

The momentum equations with an added turbulent viscosity reads

$$\frac{\partial \bar{u}_i}{\partial t} + \frac{\partial \bar{u}_j \bar{u}_i}{\partial x_j} = \delta_{1i} - \frac{1}{\rho} \frac{\partial \bar{p}}{\partial x_i} + \frac{\partial}{\partial x_j} \left((v + v_t) \frac{\partial \bar{u}_i}{\partial x_j} \right) \quad (1)$$

where the first term on the right side is the driving pressure gradient in the streamwise direction, which is used only in the channel flow simulations.

2.2. The LRN PANS k – ε turbulence model

The low-Reynolds number partially averaged Navier–Stokes (LRN PANS) turbulence model reads ([Ma et al., 2011](#))

$$\begin{aligned} \frac{\partial k}{\partial t} + \frac{\partial \bar{u}_j k}{\partial x_j} &= \frac{\partial}{\partial x_j} \left[\left(v + \frac{v_t}{\sigma_{ku}} \right) \frac{\partial k}{\partial x_j} \right] + P_k - \varepsilon \\ \frac{\partial \varepsilon}{\partial t} + \frac{\partial \bar{u}_j \varepsilon}{\partial x_j} &= \frac{\partial}{\partial x_j} \left[\left(v + \frac{v_t}{\sigma_{\varepsilon u}} \right) \frac{\partial \varepsilon}{\partial x_j} \right] + C_{\varepsilon 1} f_1 P_k \frac{\varepsilon}{k} - C_{\varepsilon 2}^* \frac{\varepsilon^2}{k} \\ P_k &= v_t \left(\frac{\partial \bar{u}_i}{\partial x_j} + \frac{\partial \bar{u}_j}{\partial x_i} \right) \frac{\partial \bar{u}_i}{\partial x_j}, \quad C_{\varepsilon 2}^* = C_{\varepsilon 1} + \frac{f_k}{f_\varepsilon} (C_{\varepsilon 2} f_2 - C_{\varepsilon 1}) \\ v_t &= C_\mu f_\mu \frac{k^2}{\varepsilon}, \quad \sigma_{ku} \equiv \sigma_k \frac{f_k^2}{f_\varepsilon}, \quad \sigma_{\varepsilon u} \equiv \sigma_\varepsilon \frac{f_\varepsilon^2}{f_k}, \quad \sigma_k = 1.4, \quad \sigma_\varepsilon = 1.4 \\ C_{\varepsilon 1} &= 1.5, \quad C_{\varepsilon 2} = 1.9, \quad C_\mu = 0.09, \quad f_\varepsilon = 1 \end{aligned} \quad (2)$$

where the damping functions are defined as

$$\begin{aligned} f_2 &= \left[1 - \exp \left(-\frac{y^*}{3.1} \right) \right]^2 \left\{ 1 - 0.3 \exp \left[-\left(\frac{R_t}{6.5} \right)^2 \right] \right\} \\ f_\mu &= \left[1 - \exp \left(-\frac{y^*}{14} \right) \right]^2 \left\{ 1 + \frac{5}{R_t^{3/4}} \exp \left[-\left(\frac{R_t}{200} \right)^2 \right] \right\} \end{aligned}$$

At walls, $k = 0$ is specified. For the dissipation rate, ε , the value at the adjacent wall nodes with a wall distance of y is prescribed as

$$\varepsilon = 2\nu \frac{k}{y^2} \quad (3)$$

For the hump flow, it was found that this boundary condition for ε gave numerical problems. Instead, ε was computed as in the one-equation hybrid LES–RANS model ([Davidson, 2009](#))

$$\varepsilon = \frac{k^{3/2}}{\ell}, \quad \ell = \kappa C_\mu^{-3/4} y [1 - \exp(-0.2k^{1/2}y/\nu)] \quad (4)$$

with $\kappa = 0.41$.

Based on the discussion in Section 1, a baseline value of $f_k = 0.4$ is chosen. The range of $0.2 < f_k < 0.6$ is evaluated. Furthermore, a variable $f_k = C_\mu^{-1/2}(\Delta/L_t)^{2/3}$ is used, see Section 4.1, as suggested by [Girimaji and Abdol-Hamid \(2005\)](#) and [Basara et al. \(2011\)](#).

The Reynolds number is high in the test cases evaluated in the present study. This means that the cut-off length scale is in the inertial subrange, so that the subgrid dissipation is equal to the viscous dissipation. Hence the f_ε is set to one, i.e. $f_\varepsilon = 1$ ([Lakshmipathy et al., 2011](#)).

The key element in the present use of the PANS model is that the $C_{\varepsilon 2}^*$ coefficient includes f_k . When f_k in the $C_{\varepsilon 2}^*$ coefficient is equal to one, the model acts as a standard k – ε model. When f_k is decreased to, say, 0.4, the destruction term is decreased, which increases ε . This reduces the modeled turbulent kinetic energy, k , and the turbulent viscosity and the model switches to an SGS (subgrid-scale) model.

It may be noted that the PANS model is very similar to the PITM model ([Schiestel and Dejoan, 2005](#); [Chaouat and Schiestel, 2005](#)). In the PITM model, the expression for $C_{\varepsilon 2}$ is the same as in the PANS model with $f_\varepsilon = 1$

$$C_{\varepsilon 2}^{\text{PITM}} = \frac{3}{2} + \frac{k}{k + k_{\text{res}}} \left(C_{\varepsilon 2} - \frac{3}{2} \right) = C_{\varepsilon 1} + f_k (C_{\varepsilon 2} - C_{\varepsilon 1}) \quad (5)$$

where k_{res} denotes the resolved turbulence. The final expressions used (Schiestel and Dejoan, 2005; Chaouat and Schiestel, 2005) involve the ratio of the filter width to the integral length scale where the latter is taken as a fraction of the wall distance. However, the diffusion coefficients in the k and ε equations are not modified in PITM. The use of f_k in the diffusion coefficient implies that the diffusion transport of k and ε is related to a RANS viscosity rather than to an SGS viscosity (Ma et al., 2011). The inclusion of f_k in the diffusion of k and ε was found to be negligible in the present channel flow simulations (see Section 4.1) as well as in hump flow simulations (Davidson and Peng, 2011, 2013) and in hill flow simulations (Ma et al., 2011). The influence on the modeled viscosity was non-negligible in the latter two flows, but the resolved turbulence was much larger than the modeled one leading to negligible difference in the mean flows.

2.2.1. The interface conditions

The interface plane separates the URANS region near the wall and the LES region in the outer region. In the former region, the turbulent viscosity, ν_t , should be a RANS viscosity and in the latter region it should be an SGS viscosity. Hence ν_t must decrease rapidly when going from the URANS region to the LES region. This is achieved by setting the usual convection and diffusion fluxes of k at the interface to zero. New fluxes are introduced in which the interface condition is set to $k_{int} = f_k k_{RANS}$, where k_{RANS} is the k value in the cell located in the URANS region adjacent to the interface. Unless otherwise stated, no modification is made for the convection and diffusion of ε across the interface. The implementation is presented in some detail below. We write the discretized equation in the y direction (see Figs. 1 and 2) as (Versteegh and Malalasekera, 1995)

$$a_P k_P = a_N k_N + a_S k_S + S_U, \quad a_P = a_S + a_N - S_P$$

where a_S and a_N are related to the convection and diffusion through the south and north face, respectively, and S_U and $S_P k_P$ include the production and the dissipation term, respectively. For a cell in the LES region adjacent to the interface (cell P), a_S is set to zero, setting the usual convection and diffusion fluxes to zero. New fluxes, including f_k , are incorporated in additional source terms as

$$S_U = (C_s + D_s) f_k k_S, \quad S_P = -(C_s + D_s) \quad (6)$$

$$C_s = \max(\bar{v}_s A_s, 0), \quad D_s = \frac{\mu_{tot} A_s}{\Delta y}$$

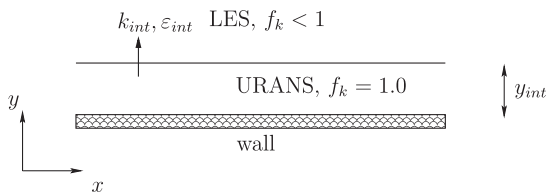


Fig. 1. The URANS and the LES regions.

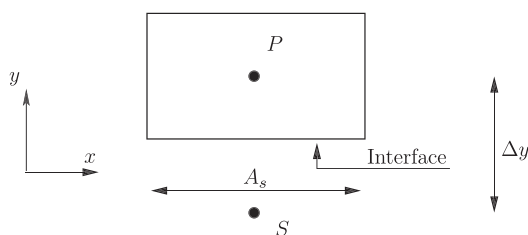


Fig. 2. Control volume, P , in the LES region adjacent to the interface.

where C_s and D_s denote convection (first-order upwind) and diffusion, respectively, through the south face, and A_s is the south area of the cell. As can be seen, the k_S is multiplied by f_k and hence the new convective flux is a factor f_k smaller than the original one. Also the diffusion flux is smaller; it is $D_s(f_k k_S - k_P)$ compared with the original flux $D_s(k_S - k_P)$.

The interface is in the present work defined along gridlines. The approach presented above is also applicable when the location is automatically computed where the extent of the RANS region varies along the wall. The convective and diffusive fluxes are modified in exactly the same way.

The present method of adding a new flux in the k equation is similar to the method proposed in Girimaji and Wallin (2013). In that work they take into account the spatial variation of f_k . A decrease of f_k in space – as occurs at the interface in Fig. 1 – means that the turbulent kinetic energy should be transferred from modeled to resolved. This is done by introducing a source term in the k equation which decreases the turbulent viscosity. Girimaji and Wallin (2013) also add a turbulent diffusion term in the momentum equation which appears as a source term in the equation for turbulent resolved kinetic energy. No source term is used in the momentum equations in the present method. A further difference is that the present method modifies the equations only in the LES region (in which k is reduced), not in the RANS region. The reason is that this effect is believed to be the most critical; it is important that the resolved turbulence on the LES side of the interface is activated as soon as possible (i.e. as close as possible to the interface). The total turbulent kinetic energy across the interface is not conserved in the present method, but as shown below, the total turbulent kinetic energy that is lost across the interface is not large.

3. Numerical method

An incompressible, finite volume code is used (Davidson and Peng, 2003). The numerical procedure is based on an implicit, fractional step technique with a multigrid pressure Poisson solver and a non-staggered grid arrangement. For the momentum equations, central differencing is used in space in the channel flow simulations; in the hump flow simulations 5% upwinding is employed using the second-order van Leer (1974) scheme.

For both flows, the Crank–Nicolson scheme is used in the time domain and the first-order hybrid central/upwind scheme is used in space for solving the k and ε equations.

This numerical method has been shown to give accurate results for DNS of channel flow at $Re_\tau = 500$ with a $64 \times 64 \times 64$ mesh (Davidson and Billson, 2006).

4. Results

4.1. Channel flow

Fully developed channel flow is computed for Reynolds numbers $Re_\tau = u_\tau \delta / \nu = 4000, 8000, 16,000$ and $32,000$, where δ denotes half channel width. The baseline mesh has 64×64 cells in the streamwise (x) and spanwise (z) directions, respectively. The size of the domain is $x_{max} = 3.2, y_{max} = 2$ and $z_{max} = 1.6$. A simulation with twice as large domain in the x – z plane ($x_{max} = 6.4$ and $z_{max} = 3.2$) with 128×128 cells was also made for $Re_\tau = 4000$, and identical results were obtained as for the smaller domain. The number of cells in the y direction varies between 80 and 128 cells depending on the Reynolds number, see Table 1. The baseline position for the interface is at $y^+ \approx 500$ for all grids unless otherwise stated.

The velocity profiles and the shear stresses are presented in Fig. 3. As can be seen, the predicted velocity profiles are in good

Table 1Grids, $f_y = 1.15$ (stretching).

Re_τ	Δy^+	Δx^+	Δz^+	N_y
4000	2.2–520	200	100	80
8000	1.5–1050	400	200	96
16,000	0.3–2100	800	400	128
32,000	0.6–4200	1600	800	128

agreement with the log-law. Fig. 3b presents the resolved shear stresses. The interface is shown by thick dashed vertical lines; it moves towards the wall for increasing Reynolds number since it is located at $y^+ \simeq 500$ for all Reynolds numbers. In the same way, the region where the modeled and viscous shear stresses are important decreases for increasing Reynolds number, see Fig. 3c.

Figs. 4 and 5 present the velocity and shear stress profiles on coarse meshes (half as fine in x and z) and fine meshes (twice as fine in x and z), respectively. The results are almost the same as on the baseline mesh (the velocity profile on the coarse mesh for the highest Reynolds number is slightly worse).

In the region of the interface, the contribution of both the resolved and the modeled shear stresses are significant. This raises the question whether the total turbulent kinetic energy might be overpredicted in this region. Fig. 6 shows how the modeled, resolved and total turbulent kinetic energy vary for different Reynolds numbers. As can be seen, the total turbulent kinetic energy (Fig. 6b) agrees fairly well with DNS data at $Re_\tau = 2000$, except for the highest Re numbers for which it is strongly overpredicted near the wall.

Fig. 7 presents how the kinetic energies vary across the interface. As can be seen, the sum of the modeled and turbulent kinetic energy show a nonphysical drop when going from the RANS region to the LES region (Fig. 7a). The reason for this drop is the sharp drop in the modeled kinetic energy (see the lines at the bottom of Fig. 7a). The total kinetic energy (Fig. 7b) exhibits a monotonic increase with y , but there is a small reduction in the gradient across the interface. As mentioned in Section 2.2.1, the turbulent kinetic is in the present approach not conserved across the interface. One way to improve the conservation of the total turbulent kinetic energy could be to add resolved kinetic energy on the LES side as proposed by Girimaji and Wallin (2013).

It was shown in Yakhot et al. (2010) that the turbulent kinetic energy should be independent of Reynolds number provided that $Re_{2h} > 10^5$ ($Re_\tau \gtrsim 2000$). Fig. 6 shows that this is well satisfied in the outer region ($y > 0.1$) where the total kinetic energies also agree nicely with DNS data.

Fig. 8 compares the baseline PANS with RANS ($f_k = 1$ everywhere). The modeled content in the URANS region with zonal PANS is very small compared to what is seen in steady RANS. Why is this so? In the URANS region, the PANS model is operating in full RANS mode, i.e. $f_k = 1$. As expected, the RANS simulation gives a much larger turbulent viscosity in the LES region than the PANS simulation does. But as can be seen, this is also true for the URANS region. The dissipations for the PANS simulation and the RANS simulation are very similar in the URANS region, see Fig. 8c. The reason for the low modeled content in the URANS region when using PANS is the low modeled turbulent kinetic energy, see Fig. 8b. The low k values are created by the interface condition in Eq. (6): the instantaneous

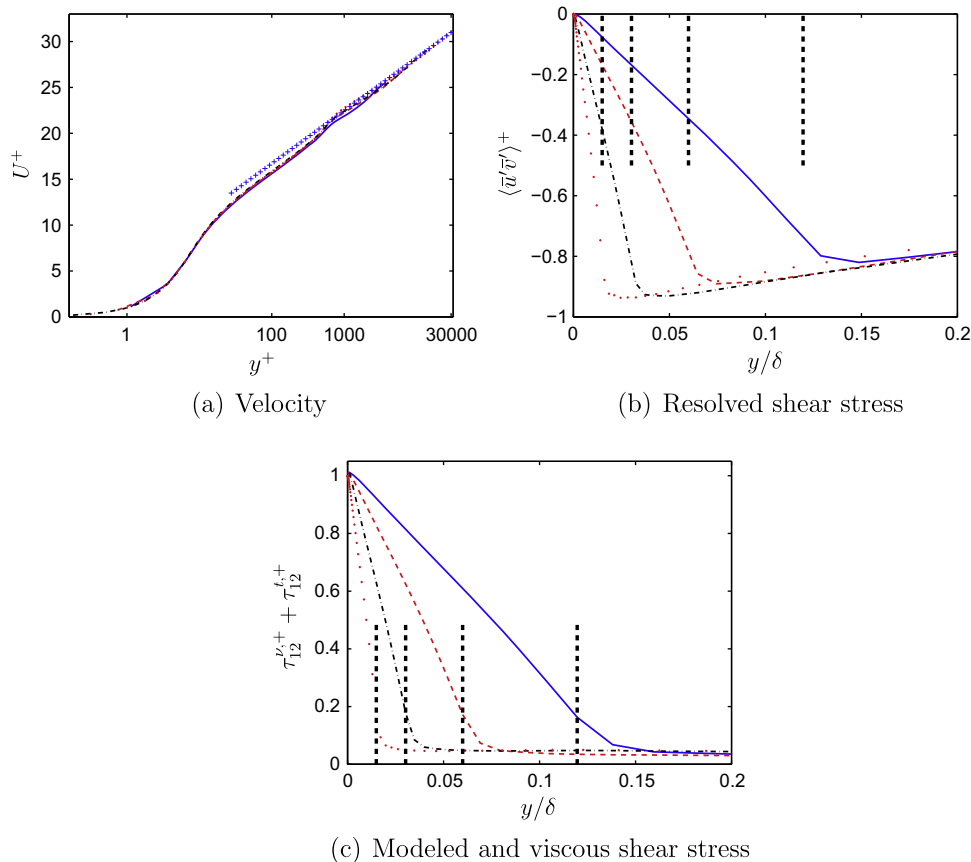


Fig. 3. Velocity and shear stress. $(N_x \times N_z) = (64 \times 64)$ —: $Re_\tau = 4000$; ---: $Re_\tau = 8000$; ···: $Re_\tau = 16,000$; -·-·: $Re_\tau = 32,000$. Vertical thick dashed lines show the interface line between the URANS and the LES region.

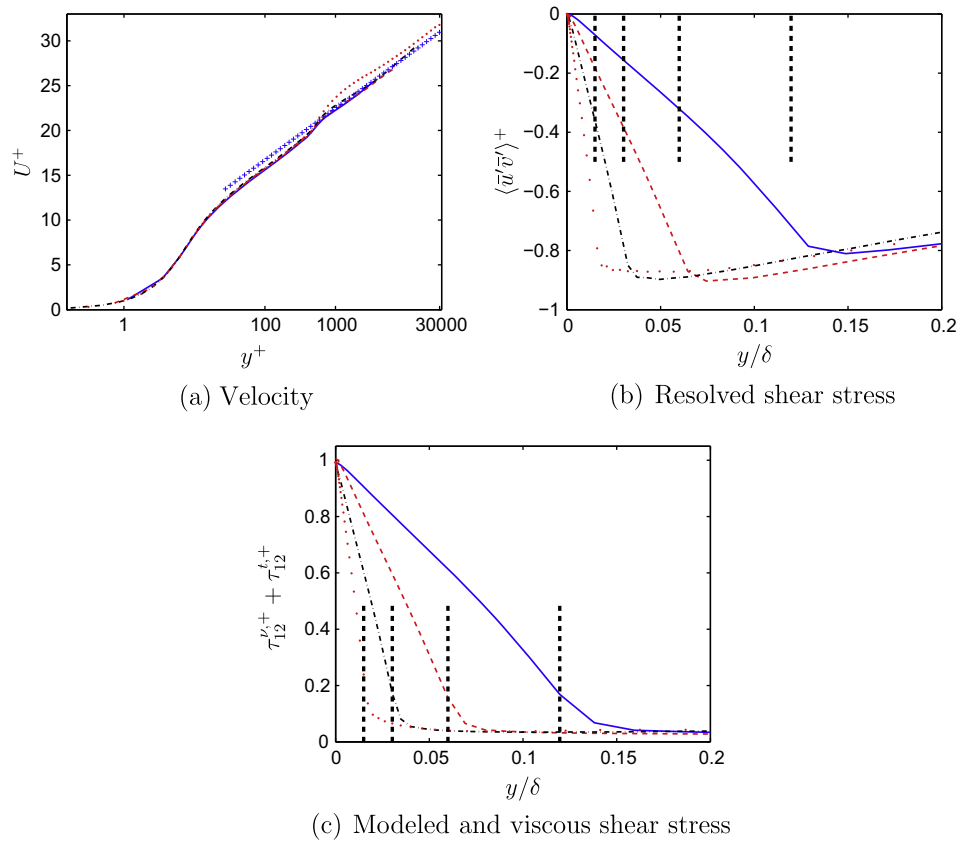


Fig. 4. Velocity and shear stress. $(N_x \times N_z) = (32 \times 32)$. For legend, see Fig. 3.

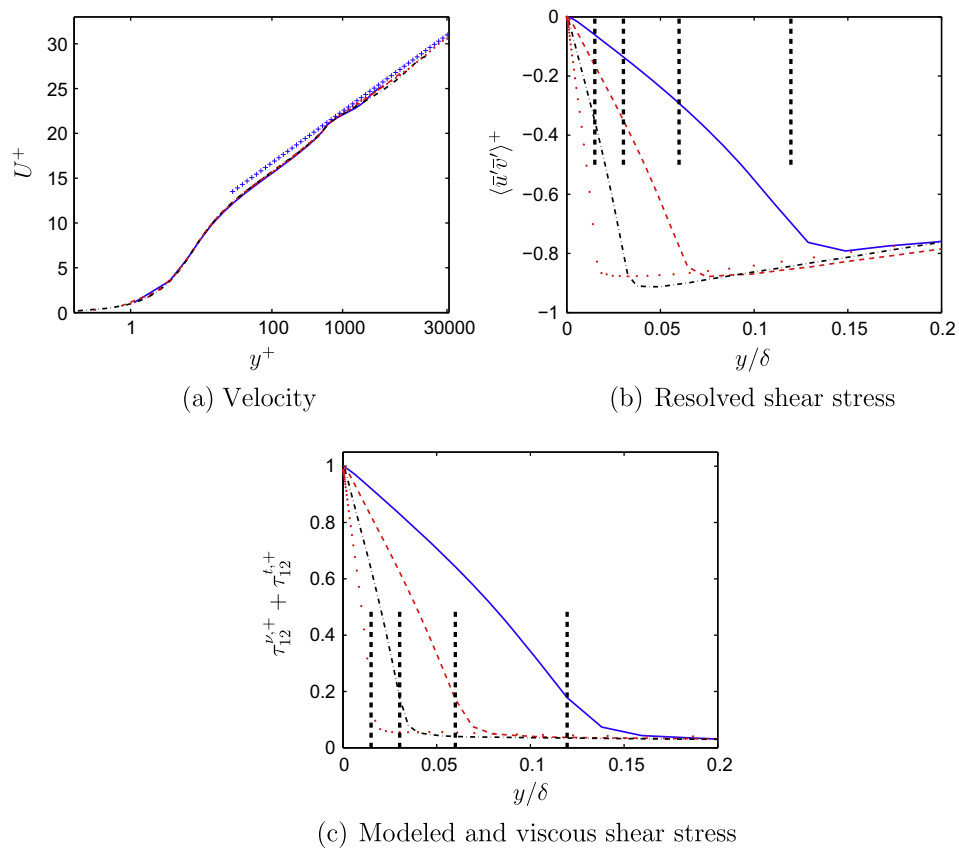


Fig. 5. Velocity and shear stress. $(N_x \times N_z) = (128 \times 128)$. For legend, see Fig. 3.

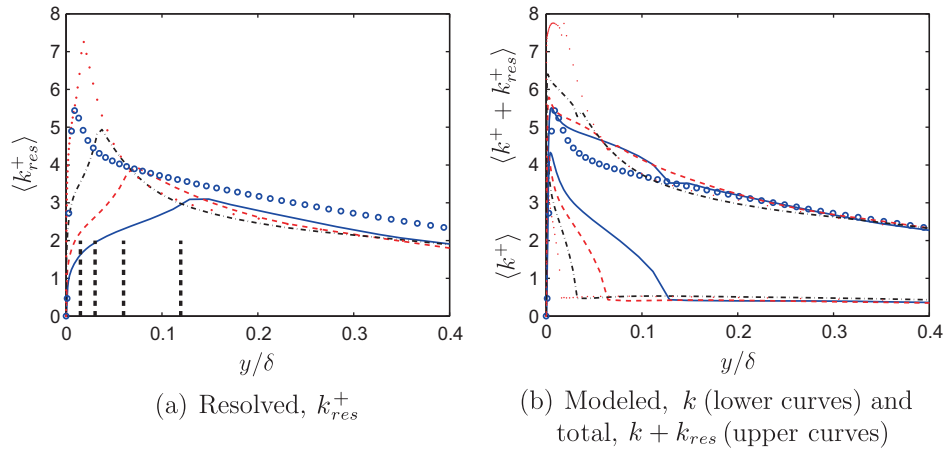


Fig. 6. Turbulent kinetic energies. $(N_x \times N_z) = (64 \times 64)$. For legend, see Fig. 3. \circ : DNS at $Re_\tau = 2000$ (Hoyas and Jiménez, 2006).

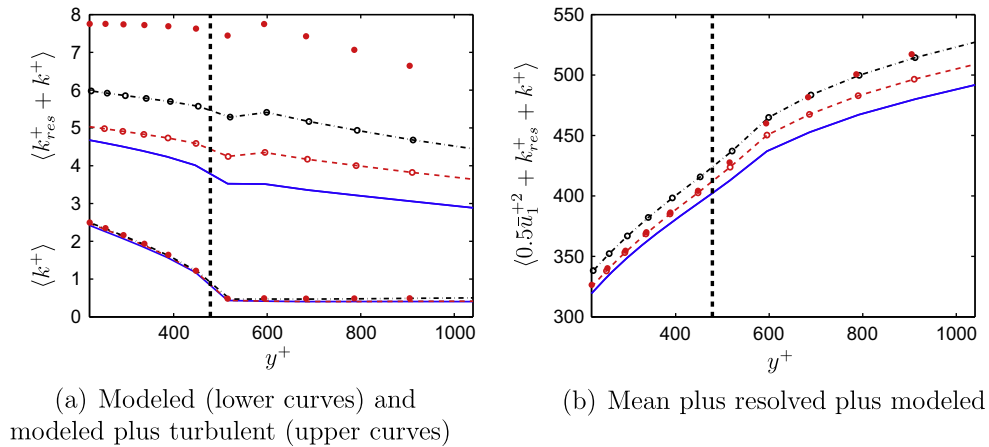


Fig. 7. Kinetic energies near the interface. $(N_x \times N_z) = (64 \times 64)$. For legend, see Fig. 3. Markers show the computational cell centers. The vertical thick dashed lines show the location of the interface.

convection of k (the diffusion is much smaller) leaving the URANS region is reduced by a factor of f_k which reduces k in the LES region. When the instantaneous convection is in the direction towards the wall, it brings small k values into the URANS region which reduces k – and the turbulent viscosity – in the URANS region. Results of a simulation where no interface condition on k is used (i.e. Eq. (6) is not used) are also included in Fig. 8 (see also Fig. 17). This illustrates the critical influence of the interface condition. Without the interface condition, the modeled turbulent kinetic and the turbulent viscosity become too high which results in a poorly predicted velocity profile (not shown).

The baseline value of the position of the interface is $y^+ \simeq 500$. Fig. 9 presents the sensitivity to the position of the interface. The peak in the viscosity profiles is located approximately in the middle of the URANS region. It can be seen that, as the interface is moved closer to the wall, the peak of the turbulent viscosity gets smaller. At the innermost location ($y^+ = 130$), the velocity profile is poorly predicted, but, if the location is in the region of $500 < y^+ < 1000$, the velocity profile is well predicted. It is not obvious why poor results are obtained with the interface at $y^+ = 130$. It has been reported in the literature that locating the interface too close to the wall inhibits the flow on the LES side to evolve efficiently into turbulence-resolving mode. This was found in Piomelli et al. (2003) who put the interface at $y^+ = 130$ and in Davidson and Dahlström (2005) and Davidson and Billson (2006)

who defined the interface at $y^+ = 60$. Forcing at the interface was used in these works to stimulate growth of resolved turbulence on the LES side. It may be that the method proposed in Girimaji and Wallin (2013) could also act as a stimulator of resolved turbulence since they add a source in the momentum equations with the object of adding resolved turbulence.

Instantaneous velocity profiles around the interface region are shown in Fig. 10. As can be seen, the interface is sometimes visible in the profiles, sometimes not. The resolved fluctuations, \bar{u}' , are clearly visible and $\langle \bar{u}'^2 \rangle$ makes an important contribution to k_{res} in Fig. 6a.

Fig. 11 presents the effect of f_k on the predicted velocity and turbulent viscosity at $Re_\tau = 16,000$. The turbulent viscosity increases, as expected, for increasing values of f_k . The velocity profile is very well predicted with $f_k = 0.5$ and rather well with $f_k = 0.2$ and $f_k = 0.3$. For $f_k = 0.6$ the velocity profile is poorly predicted and the flow in the LES region is somewhere in between steady mode (RANS) and turbulence-resolving mode (LES); the result is a poorly turbulence-resolved flow with too large turbulent viscosity (too much damping). It is possible that the method proposed in Girimaji and Wallin (2013) or some kind of forcing (Batten et al., 2004; Piomelli et al., 2003; Davidson and Dahlström, 2005; Davidson and Billson, 2006) could induce the flow to go into turbulence-resolving mode. At $Re_\tau = 8000$ the flow goes steady on all three grids with $f_k = 0.6$ (not shown).

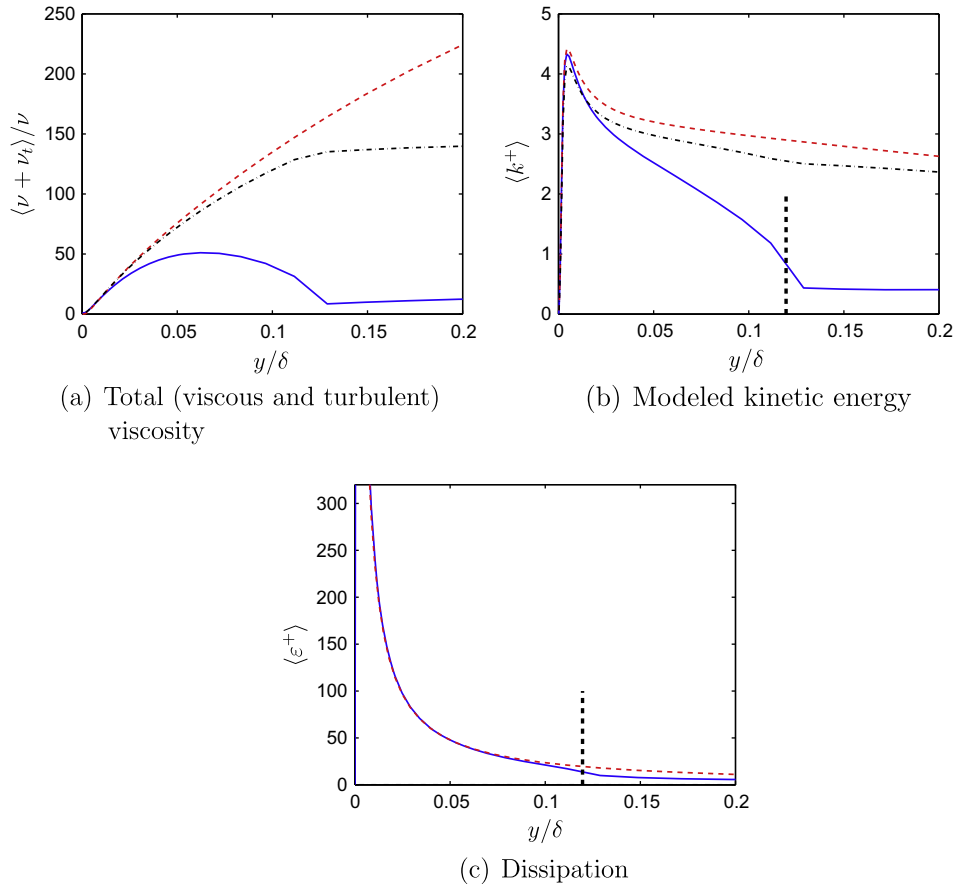


Fig. 8. Comparison between RANS ($f_k = 1$) and zonal PANS. $Re_\tau = 4000$. —: PANS (baseline case) - - - : RANS; - · - : PANS, no interface condition on k (Eq. (6) is not used). Vertical thick dashed lines show the interface line between the URANS and the LES region.

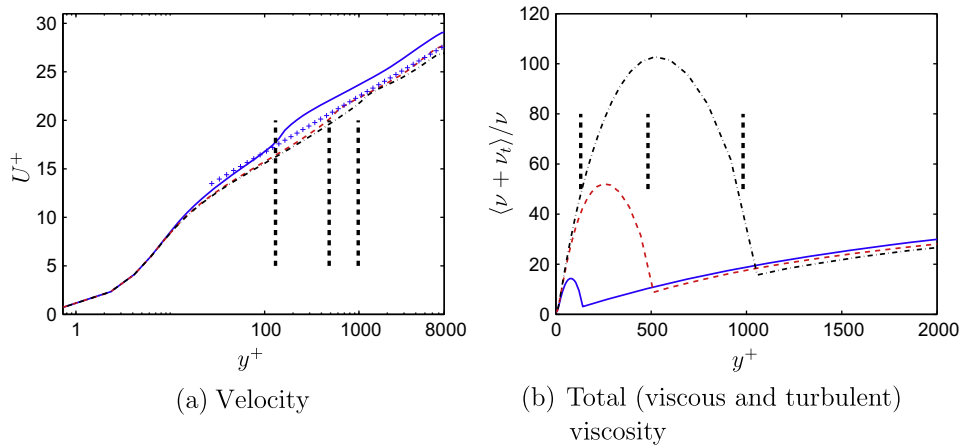


Fig. 9. Velocity and total viscosity. $Re_\tau = 8000$. Interface location at —: $y^+ = 130$ - - - : $y^+ = 500$ - · - : $y^+ = 980$.

The turbulent viscosity profiles are shown in Fig. 12 for three different resolutions in the x – z plane. It is interesting to note that the turbulent viscosity is not affected by the grid resolution. Hence, the model yields *grid independent* results. Note that the ratio of the filter width, $\Delta = (\Delta V)^{1/3}$, on the fine grid (128×128) to that on the coarse (32×32) grid is $16^{1/3} \approx 2.5$. Hence, an SGS model based on Δ would give a 2.5 larger viscosity on the coarse mesh than on the fine mesh. The same effect was seen in hump flow simulations carried out by Davidson and Peng (2011, 2013) using PANS

($f_k = 0.4$ everywhere); a grid refinement (doubling the number of cells in the spanwise direction) gave no reduction in the turbulent viscosity.

It can be seen that the turbulent viscosity (Fig. 12) is sharply reduced when moving across the interface from the URANS region to the LES region. This is achieved by the modified interface convection and diffusion fluxes in the k equation, see Eq. (6). This is an essential feature of the present approach (see Fig. 8) since the small viscosity on the LES side of the interface is helpful in stimulating a

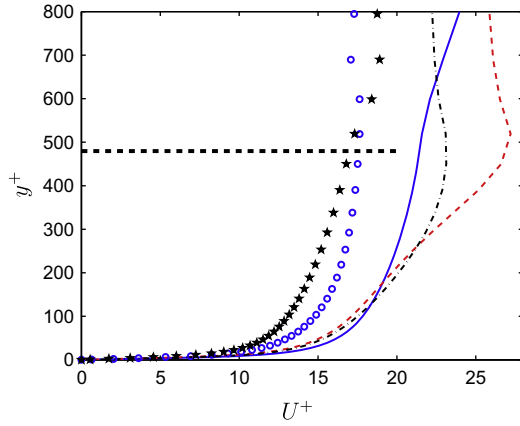


Fig. 10. Instantaneous velocity profiles. $Re_\tau = 8000$. The horizontal dashed thick line shows the interface.

rapid growth of resolved turbulence, thereby promoting the transition from modeled mode (RANS) to turbulence-resolving mode (LES).

In Section 1 it was mentioned that the inclusion of f_k in the turbulent diffusion coefficient for k and ε has a negligible effect. This is shown in Fig. 13 in which the turbulent viscosity is presented (there is no effect on the mean flow). When $\sigma_k = \sigma_{ku}$ and $\sigma_\varepsilon = \sigma_{\varepsilon u}$ the diffusion of k and ε decreases by a factor of six when $f_k = 0.4$ (see Eq. (2)) compared to the baseline PANS model. The result is that the peaks in k and ε (and hence also ν_t) are less smeared out compared to the baseline model. This was also seen in hill flow simulations (Ma et al., 2011).

It is shown in Fig. 12 that the turbulent viscosity is independent of the grid. The production term, $\langle P_k \rangle$, also stays fairly constant when the grid is refined or coarsened, see Fig. 14, at least for $y/\delta \gtrsim 0.3$. As expected, the k equation is in the LES region in local equilibrium, i.e.

$$\langle P_k \rangle = \langle \varepsilon \rangle \quad (7)$$

see Fig. 15a. Interestingly, the time-averaged production and destruction terms in the ε equation are in the LES region also in balance, see Fig. 15b, i.e.

$$\left\langle C_{\varepsilon 1} \frac{\varepsilon}{k} P_k \right\rangle - \left\langle C_{\varepsilon 2} \frac{\varepsilon^2}{k} \right\rangle + \langle D^\varepsilon \rangle \simeq \left\langle C_{\varepsilon 1} \frac{\varepsilon}{k} P_k \right\rangle - \left\langle C_{\varepsilon 2} \frac{\varepsilon^2}{k} \right\rangle = 0 \quad (8)$$

where D^ε denotes diffusion of ε (the time-averaged convection, $\langle C^\varepsilon \rangle = 0$). The diffusion term, D^ε , is entirely negligible in the LES region (not shown). It seems that both relations in Eqs. (7) and (8) cannot be satisfied since $C_{\varepsilon 1} \neq C_{\varepsilon 2}^*$. It is found that the instantaneous convective terms in the k and the ε equations are of the same order as the production and dissipation terms (although the time average of the convective terms is zero), see Fig. 15. Hence, instantaneously, the production, destruction and convection terms are the important terms in the k and the ε equations, but when the equations are time-averaged the production and destruction terms balance each other.

But one question remains: how can the *time-averaged* production and destruction terms in *both* the k and ε equations (Eqs. (7) and (8)) be in balance? The reason is that although

$$C_{\varepsilon 1} \frac{\langle \varepsilon \rangle}{\langle k \rangle} \langle P_k \rangle \neq C_{\varepsilon 2}^* \frac{\langle \varepsilon \rangle^2}{\langle k \rangle} \quad (9)$$

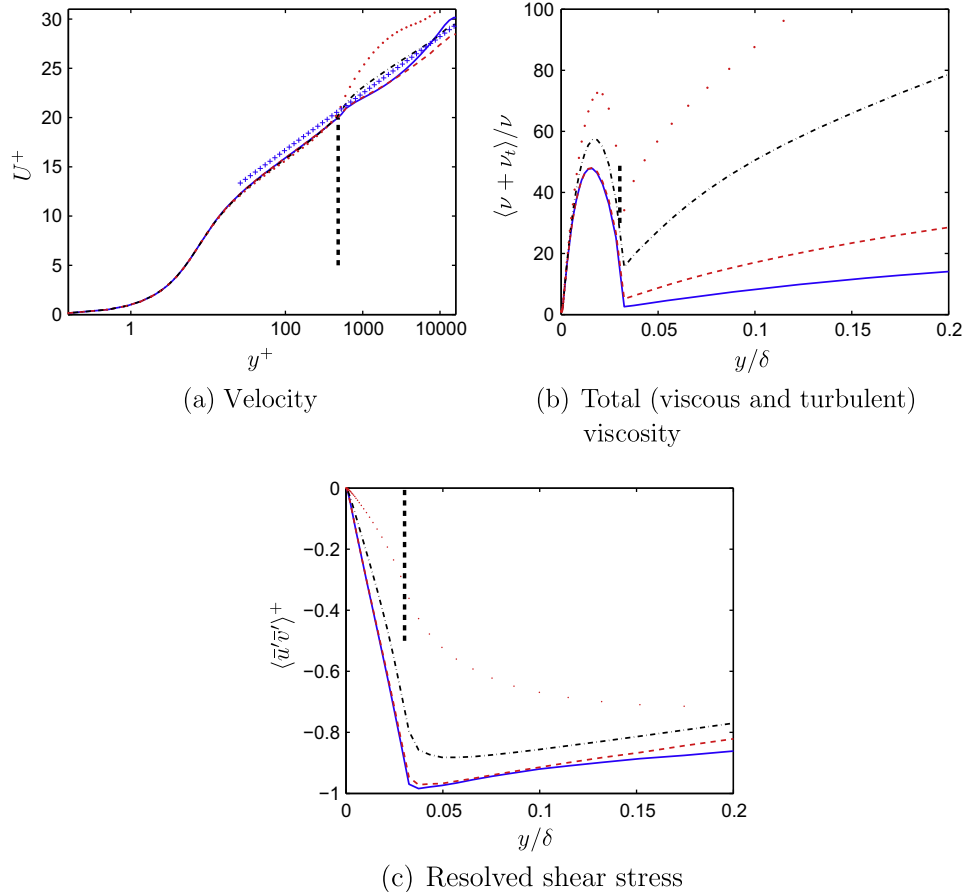


Fig. 11. Velocity, total viscosity and resolved shear stress. $Re_\tau = 16,000$. Influence of f_k . —: $f_k = 0.2$ - - - : $f_k = 0.3$ ···· : $f_k = 0.5$ ····· : $f_k = 0.6$.

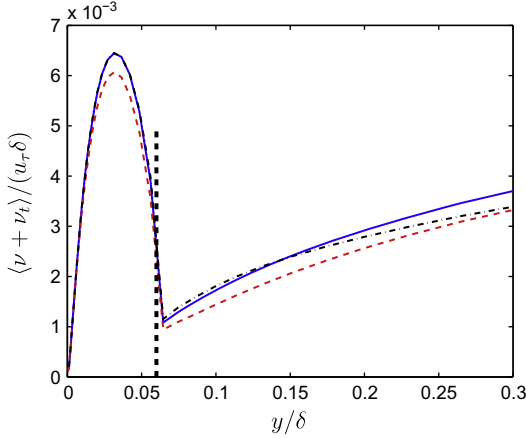


Fig. 12. Total (viscous and turbulent) viscosity. $Re_\tau = 8000$. —: $(N_x \times N_z) = (64 \times 64)$; ---: $(N_x \times N_z) = (32 \times 32)$; -.-: $(N_x \times N_z) = (128 \times 128)$.

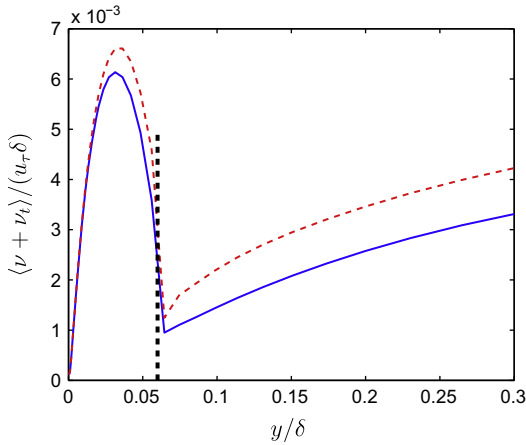


Fig. 13. Total viscosity. $Re_\tau = 8000$. $(N_x \times N_z) = (32 \times 32)$; —: σ_{ku} and σ_{eu} from Eq. (2); ---: $\sigma_{ku} = \sigma_k$ and $\sigma_{eu} = \sigma_e$.

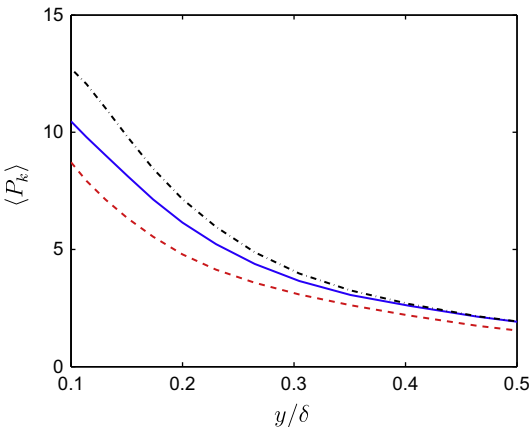


Fig. 14. Production term, P_k . $Re_\tau = 8000$. —: $(N_x \times N_z) = (64 \times 64)$; ---: $(N_x \times N_z) = (32 \times 32)$; -.-: $(N_x \times N_z) = (128 \times 128)$.

(because $\langle P_k \rangle = \langle \varepsilon \rangle$ and $C_{e1} \neq C_{e2}^*$, Fig. 15b shows that

$$C_{e1} \left\langle \frac{\varepsilon}{k} P_k \right\rangle = C_{e2}^* \left\langle \frac{\varepsilon^2}{k} \right\rangle \quad (10)$$

It is a general feature of any two (or three as in Eq. (10)) fluctuating quantities, $A = \langle A \rangle + A'$ and $B = \langle B \rangle + B'$, that $\langle AB \rangle \neq \langle A \rangle \langle B \rangle$. In the case of Eq. (10), the correlation between ε, k^{-1} and P_k (left side) is stronger than that between ε^2 and k^{-1} (right side), as shown in Fig. 16.

No special treatment was used for the ε equation at the interface in the simulations presented above. Initially, simulations were made in which the convection and the diffusion in the ε equation were modified in the same way as for the k equation, see Eq. (6). The ε value that was transported from the URANS region to the LES region was set from the Smagorinsky model in the same way as in embedded LES (Davidson and Peng, 2011, 2013)

$$\varepsilon_S = C_\mu^{3/4} k_S^{3/2} / \ell_{sgs}, \quad \ell_{sgs} = C_s \Delta \quad (11)$$

where $\Delta = (\Delta V)^{1/3}$, and ΔV is the volume of the cell adjacent to the interface. A value of $C_s = 0.07$ was found to be suitable for embedded LES (Davidson and Peng, 2011, 2013). Fig. 17 presents simulations using different values of C_s . The results when using

- no interface for ε , interface condition for k
- no interface condition for k and ε

are also included for reference. First, it can be noted that when using no interface condition in the k equation, the turbulent viscosity in the LES region becomes much too large (Fig. 17b). As a result, all resolved turbulence is killed (Fig. 17c), and as a consequence the velocity profile is poorly predicted (Fig. 17a). A value of $C_s = 0.1$ gives good agreement with the log-law (Fig. 17a) and $C_s = 0.05$ gives almost identical results (not shown). These small C_s values succeed in strongly reducing the turbulent viscosity in the LES region adjacent to the interface. Fig. 17c shows that when a large $C_s = 0.5$ is used, the magnitude of the resolved shear becomes smaller (too small) which results in an overshoot of the velocity profile in the LES region near the interface, see Fig. 17a. When making these tests it was realized that the best and most accurate treatment of the ε equation at the interface is to do nothing at all. It turns out that a value of $C_s = 0.11$ is obtained when computing C_s from Eq. (11) when post-processing data for which no interface condition on ε was used.

Constant values of f_k were used in all predictions presented above. The f_k can also be computed as proposed in Girimaji and Abdol-Hamid (2005) and Basara et al. (2011). The smallest resolved length scale should be related to the modeled (SGS) dissipation and the modeled (SGS) turbulent viscosity. Dimensional analysis gives (cf. the Kolmogorov length scale $\eta = (\nu^3/\varepsilon)^{1/4}$)

$$\ell_{res,min} = \left(\frac{\nu_t^3}{\varepsilon_{sgs}} \right)^{1/4} = \left(\frac{\nu_t^3}{\varepsilon} \right)^{1/4} \quad (12)$$

The expression of ν_t in Eq. (2) into Eq. (12) gives

$$\ell_{res,min} = \left(\frac{C_\mu^3 k^6}{\varepsilon^3 \varepsilon} \right)^{1/4} = C_\mu^{3/4} \frac{k^{3/2}}{\varepsilon} \quad (13)$$

In eddy-viscosity models, the viscosity is estimated as the product of a turbulent velocity scale, $\mathcal{U} = u_\tau$, and a turbulent length scale, $\mathcal{L} = \mathcal{U}^3/\varepsilon = u_\tau^3/\varepsilon$. Using $u_\tau = C_\mu^{1/2} k^{1/2}$ we get

$$\nu_t = \mathcal{U} \mathcal{L} = u_\tau \frac{u_\tau^3}{\varepsilon} = u_\tau C_\mu^{3/4} \frac{k^{3/2}}{\varepsilon}$$

Hence the modeled length scale, \mathcal{L} , and the minimum resolved length scale, $\ell_{res,min}$, are equal

$$\ell_{res,min} = \mathcal{L} = C_\mu^{3/4} \frac{k^{3/2}}{\varepsilon} = C_\mu^{3/4} \frac{(f_k(k + k_{res}))^{3/2}}{\varepsilon}$$

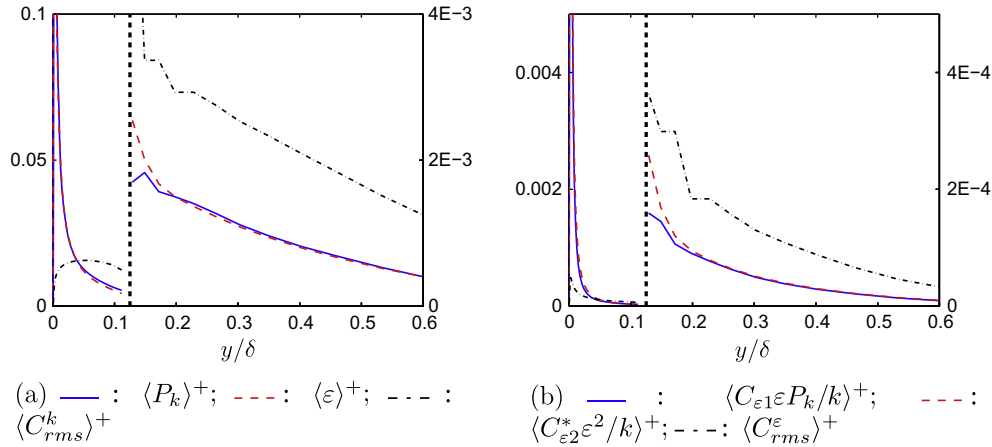


Fig. 15. Production, destruction and RMS of convection terms in the k and ε equations. Inner scaling. Left vertical axes: inner (URANS) region; right vertical axes: outer (LES) region. $Re_\tau = 4000$. $(N_x \times N_z) = (64 \times 64)$.

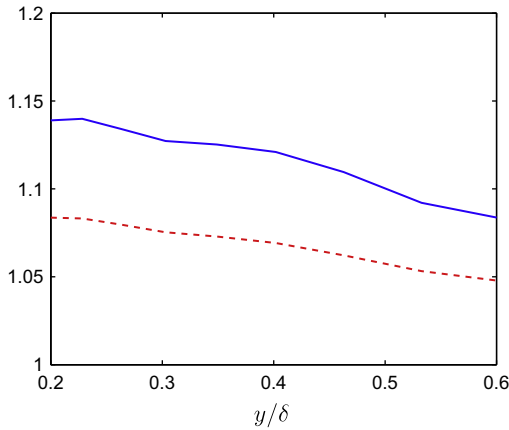


Fig. 16. Correlations of the quantities in the production and destruction terms in the ε equation. —: $\langle \frac{\partial P_k / k}{\partial y} \rangle^+$, production term; ---: $\langle \frac{\partial^2 \varepsilon / k}{\partial y^2} \rangle^+$, destruction term.

where $f_k = k/(k + k_{res})$ was used to obtain the right side. Both length scales must be larger than the grid scale, i.e. $\ell_{model} = \mathcal{L} \geq \Delta$, which give

$$f_k \geq C_\mu^{-1/2} \frac{(\Delta \varepsilon)^{2/3}}{k + k_{res}} = C_\mu^{-1/2} \left(\frac{\Delta}{L_t} \right)^{2/3}, \quad L_t = \frac{(k_{res} + k)^{3/2}}{\varepsilon}$$

This is the minimum f_k which the grid size Δ can support. If f_k is larger, we are in theory wasting some of the turbulence-resolution capability of the grid. The f_k is set from the lower limit, i.e.

$$f_k = C_\mu^{-1/2} \left(\frac{\Delta}{L_t} \right)^{2/3} \quad (14)$$

Fig. 18 shows the velocity and turbulent viscosity for different meshes when computing f_k from Eq. (14). As can be seen, the velocity profiles agree well with the log-law for the fine and the baseline meshes, but the coarse grid gives poor agreement; the turbulent viscosity becomes much too large because of a large computed f_k and as a result all resolved turbulence is killed (not shown). Hence, for the coarse grid a constant f_k is much better than computing f_k from Eq. (14).

Contrary to when constant f_k is used in the LES region, the turbulent viscosity increases when the mesh is coarsened (Fig. 18b). The reason is that f_k increases when the mesh is coarsened, see Fig. 19; for the coarse mesh $f_k = 1$ everywhere since all resolved

turbulence is killed. Fig. 19 compares f_k to the ratio $k/(k + k_{res})$. The latter is, as can be seen, much smaller than the former. Recall that the computed f_k is the minimum f_k that the grid supports, see the discussion leading to Eq. (14). The question can nevertheless be posed: what happens if f_k is computed as $f_k = k/(k + k_{res})$? Fig. 20 presents velocity and turbulent viscosity when f_k is computed in this way, but f_k is taken from the 64×64 simulation shown in Fig. 19 (i.e. f_k is constant in time and only a function of y). As can be seen, the result is poor agreement with the logarithmic law. The turbulent viscosity becomes much smaller than for the baseline case, $f_k = 0.4$, see Fig. 9.

4.2. Hump flow

As a second test case the flow over a hump is presented, see Fig. 21. The hump flow has been studied previously using LES (Avdís et al., 2009; Saric et al., 2006) and DES (Saric et al., 2006). Wall functions were used by Avdis et al. (2009), whereas the near-wall flow was resolved in Saric et al. (2006) with a refined mesh in the wall-normal directions. This flow was also studied in the ATAAC project (Schwamborn, 2012) where DES and embedded LES were used. The present author recently presented results using embedded LES (Davidson and Peng, 2011, 2013).

The Reynolds number of the hump flow is $Re_c = 936,000$, based on the hump length, c , and the inlet mean velocity at the centerline, $U_{in,c}$. Experiments are presented in Greenblatt et al. (2004, 2005). The maximum height of the hump, h , and the channel height, H , are given by $H/c = 0.91$ and $h/c = 0.128$, respectively. The baseline mesh has $312 \times 120 \times 32$ cells with $Z_{max} = 0.2c$. The grid was created by the group of Prof. Strelets in St. Petersburg and was the mandatory grid in the ATAAC project. The x – y grid is shown in Fig. 21. The interface between URANS and LES is defined at two different gridline numbers, $j = 32$ and $j = 36$ which correspond to $y^+ = 220$ and $y^+ = 380$, respectively, at the inlet. Neumann conditions are used at the outflow section located at $x/c = 4.2$. Slip conditions are used at the upper wall and symmetric boundary conditions are used on the spanwise boundaries.

In the present work embedded LES is carried out locating the inlet at $x/c = 0.6$ in the same way as in the ATAAC project and in Davidson and Peng (2011, 2013). In the ATAAC project, ANSYS Germany made embedded-LES calculation using ANSYS Fluent. The mean velocity profiles at $x/c = 0.6$ from that simulation is used as inlet boundary conditions in the present study. Anisotropic synthetic fluctuations are superimposed on the mean profiles, see Fig. 22; for details on how the synthetic fluctuations are generated,

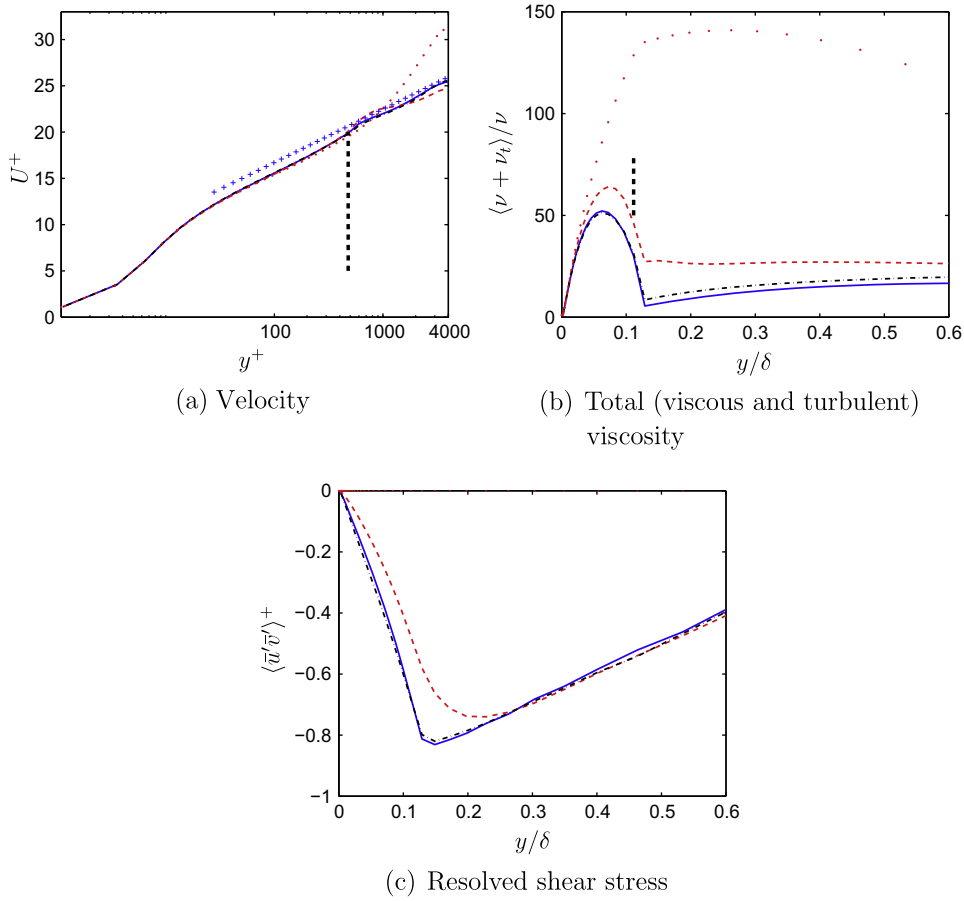


Fig. 17. Velocity, total viscosity and resolved shear stress. $Re_\tau = 4000$. $(N_x \times N_z) = (64 \times 64)$. Influence of C_s in Eq. (11). —: $C_s = 0.1$; ---: $C_s = 0.5$; ···: no interface condition on ε ; ···: no interface condition on ε or k .

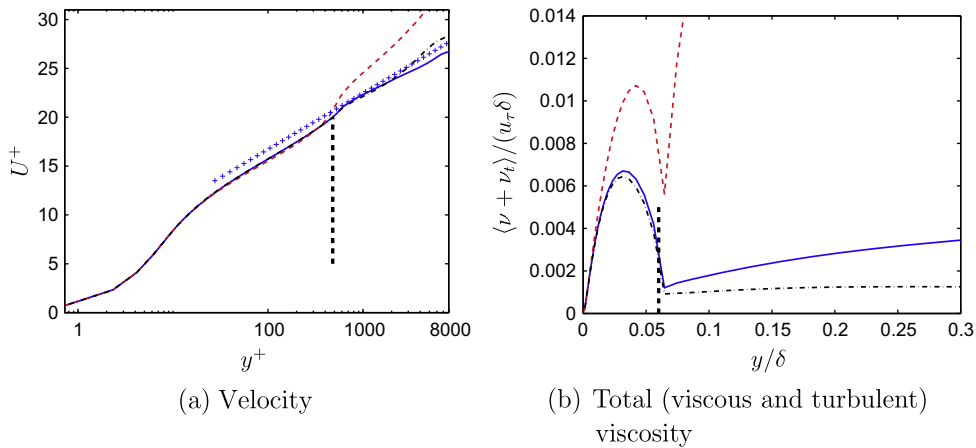


Fig. 18. Velocity and total viscosity. $Re_\tau = 8000$. f_k is computed using Eq. (14). For legend, see Fig. 14.

see Davidson (2007) and Davidson and Peng (2011, 2013). The inlet k and ε are set as

$$k_{in} = f_k k_{RANS}, \quad \ell_{sgs} = C_S \Delta \quad (15)$$

where k_{RANS} is taken from the 2D RANS simulation; for more detail, see Davidson and Peng (2011, 2013). The differences in the present work compared to the work in Davidson and Peng (2011, 2013) are:

- zonal PANS is used (in Davidson and Peng (2011, 2013) full PANS with $f_k = 0.4$ everywhere was used);

- f_k is computed in the LES region using Eq. (14) or it is set to 0.4;
- the synthetic inlet fluctuations are scaled with $(k/k_{max})_{RANS}$ (in Davidson and Peng (2011, 2013) no scaling was used);
- different mean inlet profiles;
- the mesh has only 32 cells in the spanwise direction (in Davidson and Peng (2011, 2013) 64 cells were used).

Fig. 23 compares the predicted skin friction with experiments. The agreement is good although the recirculation is slightly too weak. The predicted velocity profiles are in excellent agreement

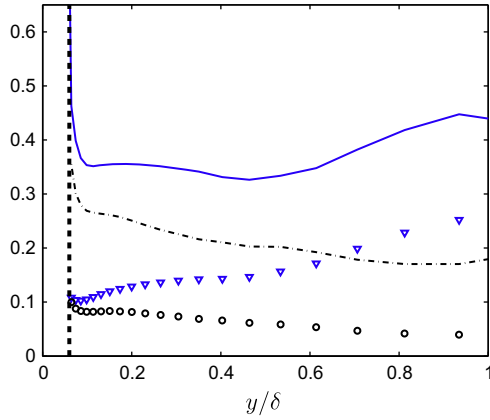


Fig. 19. f_k (Eq. (14)) and ratio of modeled to total kinetic turbulence. $Re_\tau = 8000$. —: $f_k, (N_x \times N_z) = (64 \times 64)$; - - -: $f_k, (N_x \times N_z) = (128 \times 128)$. ∇ : $k/(k + k_{res}), (N_x \times N_z) = (64 \times 64)$; \circ : $k/(k + k_{res}), (N_x \times N_z) = (128 \times 128)$.

with experiments, see Fig. 24. A small deviation between predictions and experiments can be seen near the wall for $1.0 \leq x/c \leq 1.1$. In Figs. 23 and 24 two different ways to prescribe f_k in the LES region are compared: either it is set to a constant (0.4) or it is computed using Eq. (14). As can be seen, both ways give very similar result, although the recovery rate is somewhat too slow when f_k is computed with Eq. (14).

The resolved and modeled shear stresses are presented in Fig. 25. Note that the modeled stresses are plotted with opposite sign to enhance readability. The shear stresses are somewhat over-predicted. Again, the effect of how f_k is prescribed (constant 0.4 or computed from Eq. (14)) has a very small effect. It can be seen that the modeled shear stresses are negligible. The results shown in Figs. 23–25 are as good – or slightly better – as those in Davidson and Peng (2011, 2013) although the mesh in the present work is half as fine.

Fig. 26 presents f_k and the ratio of modeled to total turbulent kinetic energy. First, it can be seen that $0.1 \leq f_k \leq 0.2$ in the turbulence-affected region (i.e. $y - y_{wall} \lesssim 0.1$), which are rather small values for LES. Second, as in the channel flow simulations (Fig. 19), the ratio $k/(k + k_{res})$ is much smaller than f_k computed from Eq. (14). It should be noted here that – as in the channel flow simulations, see Fig. 20 – if f_k were set to values corresponding to $k/(k + k_{res}) \simeq 0.01$ (see Fig. 26) all modeled turbulence would be dampened and the result would be a very poorly resolved DNS simulation.

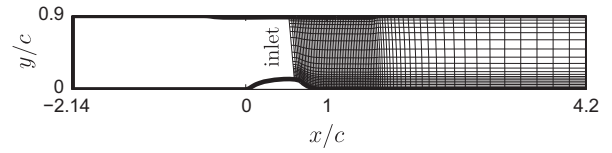


Fig. 21. Hump flow configuration and grid schematic. Every 4th grid line is shown.

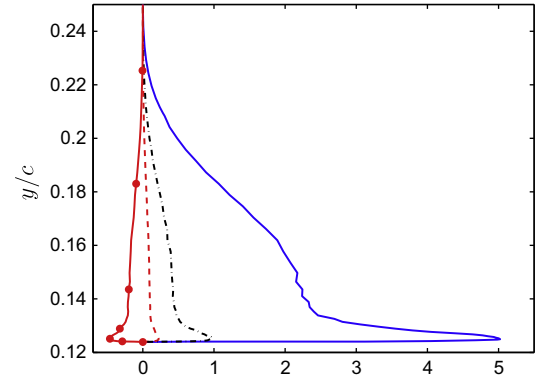


Fig. 22. Hump flow. Prescribed synthetic Reynolds stresses at the inlet. —: u_{rms}^2/u_τ^2 ; - - -: v_{rms}^2/u_τ^2 ; - · - : w_{rms}^2/u_τ^2 ; \bullet : $\langle u'v' \rangle / u_\tau^2$.

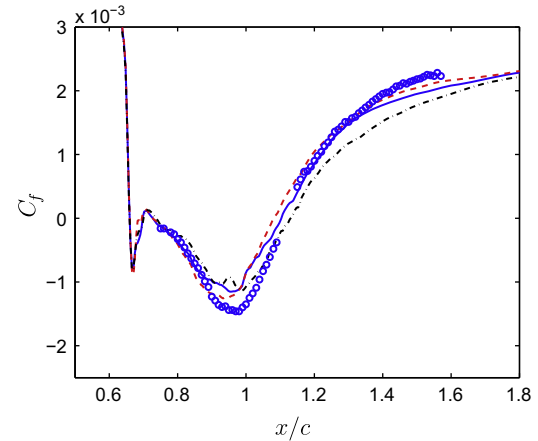
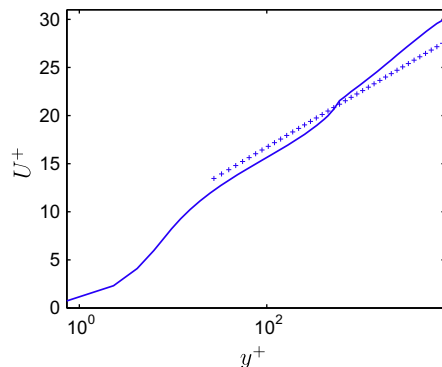
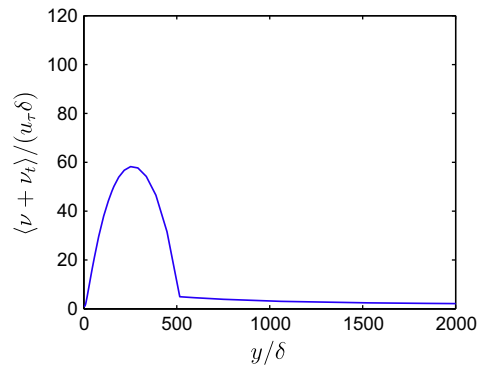


Fig. 23. Hump flow. Skin friction. —: $f_k = 0.4$, interface at $j = 36$; - - -: $f_k = 0.4$, interface at $j = 32$; - · - : f_k computed from Eq. (14), interface at $j = 36$; markers: experiments.



(a) Velocity



(b) Total (viscous and turbulent) viscosity

Fig. 20. Velocity and total viscosity. $Re_\tau = 8000$. $(N_x \times N_z) = (64 \times 64)$. In the LES region $f_k = \langle k/(k + k_{res}) \rangle$ is taken from Fig. 19.

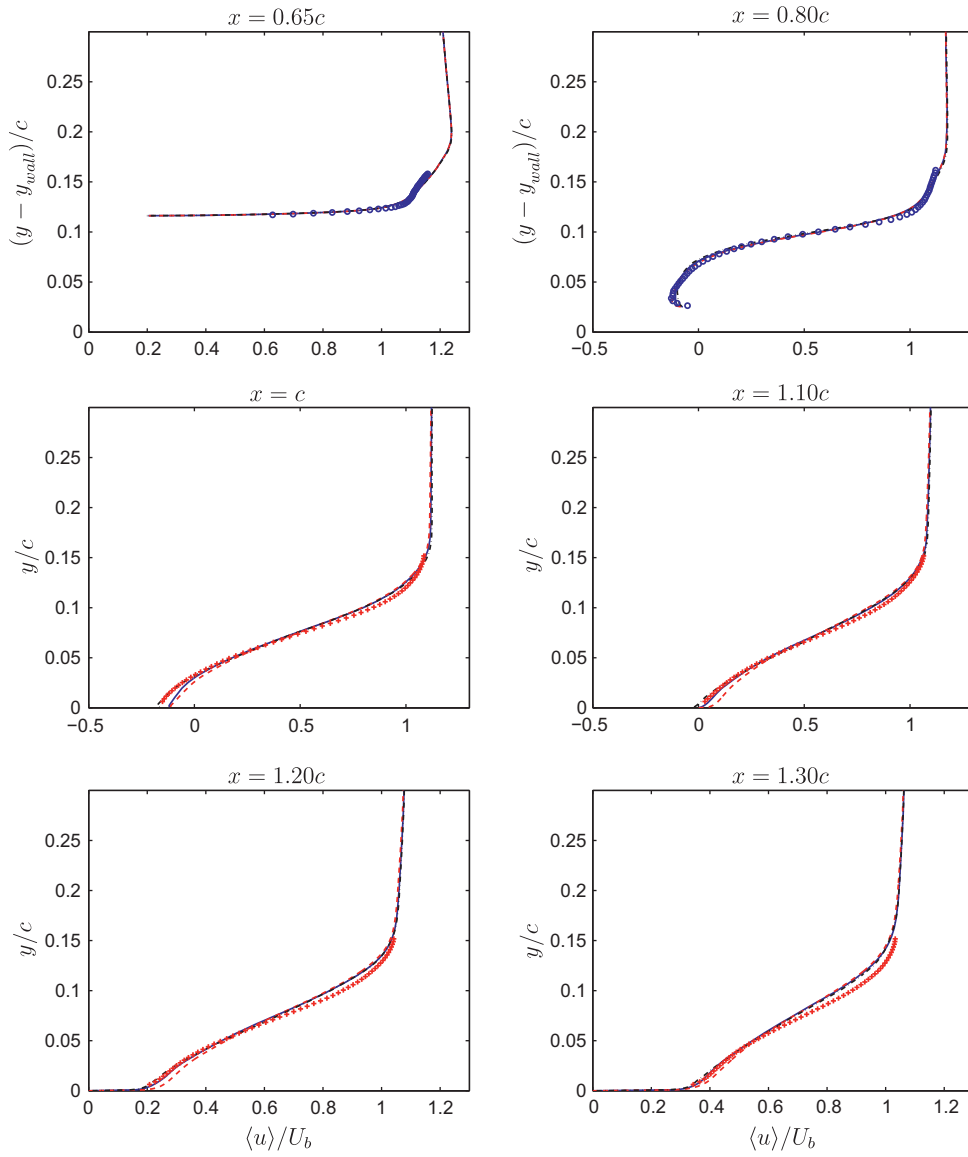


Fig. 24. Hump flow: Mean velocity, $\langle \bar{u} \rangle$. For legend, see Eq. (23). \circ : 2D PIV experiments; $+$: 3D PIV experiments.

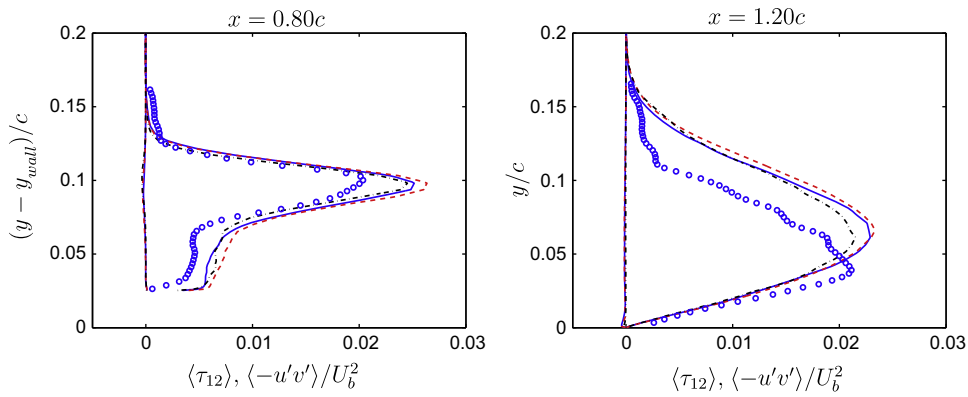


Fig. 25. Hump flow: resolved and modeled (opposite sign) turbulent shear stresses. For legend, see Fig. 24.

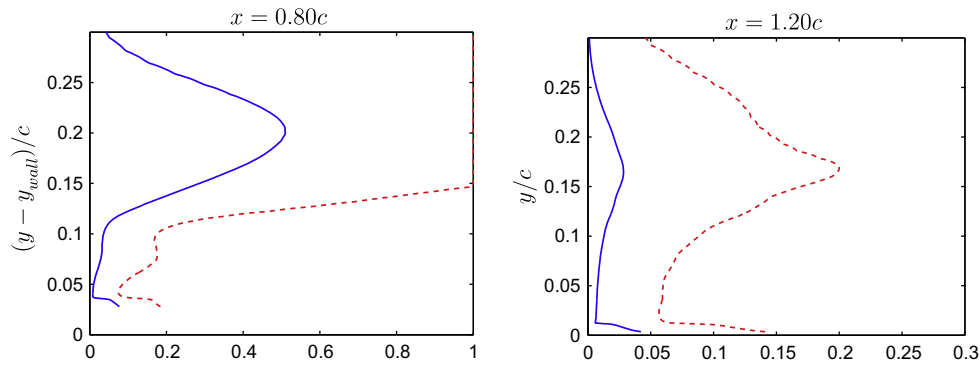


Fig. 26. Hump flow: f_k and ratio of modeled to total kinetic turbulence, f_k computed and interface at gridline $j = 36$. —: $k/(k + k_{res})$; ---: f_k computed from Eq. (14).

5. Conclusions

A new approach for using PANS as a zonal hybrid RANS–LES model has been presented. It has been evaluated for channel flow at different Reynolds numbers ($4000 \leq Re_\tau \leq 32,000$) and gives good agreement with the log-law. Furthermore, it was found that the model gives virtually grid-independent results when refining the grid in the wall-parallel planes ($N_x \times N_z = 32 \times 32, 64 \times 64$ and 128×128). When using a constant f_k , the turbulent viscosities obtained on these three grid are nearly the same. An SGS model using the cell size as a turbulent length scale would give a $16^{1/3} \approx 2.5$ smaller turbulent lengthscale on the finest mesh compared to the coarsest mesh.

The new model has also been evaluated in embedded LES for the flow over a hump. Good agreement with experiments were obtained.

Two ways are used to prescribe f_k in the LES region: either a constant value is used (baseline value 0.4 proved to be best) or it is computed as $f_k = C_\mu^{-1/2} (\Delta/L_t)^{2/3}$, see Eq. (14). The computed f_k fails on the coarse grids in the channel flow simulations; it gives much too large a turbulent viscosity which kills all resolved turbulence. In the hump flow, the constant $f_k = 0.4$ gives slightly better agreement with experiments than when computing f_k .

It was found that the ratio of modeled to total turbulent kinetic energy, $k/(k + k_{res})$, is much smaller than f_k from Eq. (14) in both flows. f_k is prescribed as $k/(k + k_{res})$ for channel flow using the baseline mesh, and it is found that the small f_k makes the modeled turbulence much too small in the LES region, see Fig. 20.

What is the advantage of using PANS in the LES region and not LES? First, if we would use a standard SGS model, such as the Smagorinsky model, in the LES region, it would be difficult to prescribe reasonable interface conditions for k and ε ; the result would be a poor prediction of the RANS region. Second, we believe that the PANS model can support coarser grids in the LES region than the Smagorinsky model. When f_k is larger than the theoretical lower limit in Eq. (14), the PANS model does indeed model a larger part of the turbulence than the Smagorinsky model.

Acknowledgements

The financial support of SNIC (the Swedish National Infrastructure for Computing) for computer time at C3SE (Chalmers Center for Computational Science and Engineering) is gratefully acknowledged. This project was financed by the EU project ATAAC (Advanced Turbulence Simulation for Aerodynamic Application Challenges), Grant Agreement No. 233710. <http://cfd.mace.manchester.ac.uk/ATAAC/WebHome>

References

- Avdiss, A., Lardeau, S., Leschziner, M., 2009. Large eddy simulation of separated flow over a two-dimensional hump with and without control by means of a synthetic slot-jet. *Flow Turb. Combust.* 83, 343–370.
- Basara, B., Krajnović, S., Girmaji, S., Pavlović, Z., 2011. Near-wall formulation of the partially averaged Navier Stokes turbulence model. *AIAA J.* 49, 2627–2636.
- Basu, D., Hamed, A., Das, K., 2007. Assessment of partially averaged Navier Stokes (PANS) multiscale model in transonic turbulent separated flows. In: 5th Joint ASME/JSME Fluids Engineering Conference, July 30–August 2, San Diego, California, USA.
- Batten, P., Goldberg, U., Chakravarthy, S., 2004. Interfacing statistical turbulence closures with large-eddy simulation. *AIAA J.* 42, 485–492.
- Chaouat, B., Schiestel, R., 2005. A new partially integrated transport model for subgrid-scale stresses and dissipation rate for turbulent developing flows. *Phys. Fluids*, 17.
- Davidson, L., 2007. Using isotropic synthetic fluctuations as inlet boundary conditions for unsteady simulations. *Adv. Appl. Fluid Mech.* 1, 1–35.
- Davidson, L., 2009. Hybrid LES–RANS: back scatter from a scale-similarity model used as forcing. *Philos. Trans. Roy. Soc. A* 367, 2905–2915.
- Davidson, L., 2012. Large eddy simulation of heat transfer in boundary layer and backstep flow using PANS. In: *Turbulence, Heat and Mass Transfer, THMT-12*. Palermo, Sicily/Italy.
- Davidson, L., Billson, M., 2006. Hybrid LES/RANS using synthesized turbulence for forcing at the interface. *Int. J. Heat Fluid Flow* 27, 1028–1042.
- Davidson, L., Dahlström, S., 2005. Hybrid LES–RANS: an approach to make LES applicable at high Reynolds number. *Int. J. Comput. Fluid Dyn.* 19, 415–427.
- Davidson, L., Peng, S.-H., 2003. Hybrid LES–RANS: a one-equation SGS model combined with a $k - \omega$ for predicting recirculating flows. *Int. J. Numer. Methods Fluids* 43, 1003–1018.
- Davidson, L., Peng, S.-H., 2011. Embedded LES with PANS. In: 6th AIAA Theoretical Fluid Mechanics Conference, 27–30 June, Honolulu, Hawaii. AIAA paper 2011-3108.
- Davidson, L., Peng, S.-H., 2013. Embedded large-eddy simulation using the partially averaged Navier–Stokes model. *AIAA J.* 51, 1066–1079.
- Egorov, Y., Menter, F., Lechner, R., Cokljat, D., 2010. The scale adaptive simulation method for unsteady flow predictions. Part 2: Application to complex flows. *Flow Turb. Combust.* 85, 139–165.
- Freund, A., Tosha, A., Girmaji, S., 2006. Flow past a backward-facing step: comparison of PANS, DES and URANS results with experiments. *Int. J. Comput. Methods Eng. Sci. Mech.* 8, 23–38.
- Fröhlich, J., von Terzi, D., 2008. Hybrid LES/RANS methods for the simulation of turbulent flows. *Prog. Aerospace* 44, 349–377.
- Girmaji, S., 2006a. Partially-averaged Navier–Stokes model for turbulence: a Reynolds-averaged Navier–Stokes to direct numerical simulation bridging method. *J. Fluids Eng.* 73, 413–421.
- Girmaji, S., 2006b. Partially-averaged Navier–Stokes model for turbulence: a Reynolds-averaged Navier–Stokes to direct numerical simulation bridging method. *ASME J. Appl. Mech.* 73, 413–421.
- Girmaji, S., Abdol-Hamid, K.S., 2005. Partially-Averaged Navier–Stokes Model for Turbulence: Implementation and Validation, Reno, NV. AIAA paper 2005-0502.
- Girmaji, S.S., Wallin, S., 2013. Closure modeling in bridging regions of variable-resolution (VR) turbulence computations. *J. Turb.* 14, 72–98.
- Greenblatt, D., Paschal, K., Yao, C.-S., Harris, J., Schaeffler, N.W., Washburn, A., 2004. A Separation Control cfd Validation Test Case. Part 1: Baseline & Steady Suction. AIAA-2004-2220.
- Greenblatt, D., Paschal, K., Yao, C.-S., Harris, J., 2005. A Separation Control cfd Validation Test Case Part 1: Zero Efflux Oscillatory Blowing. AIAA-2005-0485.
- Hoyas, S., Jiménez, J., 2006. Scaling of the velocity fluctuations in turbulent channels up to $Re_\tau = 2003$. *Phys. Fluids A* 18.
- Ji, B., Luo, X.-W., Wu, Y.-L., Xu, H.-Y., 2011. Unsteady cavitating flow around a hydrofoil simulated using the partially-averaged Navier–Stokes model. *Chin. Phys. Lett.* 29, 076401.

- Ji, B., Luo, X.-W., Wu, Y., Peng, X., XU, H., 2012. Partially-averaged Navier–Stokes method with modified $k-\varepsilon$ model for cavitating flow around a marine propeller in a non uniform wake. *Int. J. Heat Mass Transfer* 55, 6582–6588.
- Kok, J., Dol, H., Oskam, B., van der Ven, H., 2004. Extra-large Eddy Simulation of Massively Separated Flows, Reno, NV. AIAA paper 2004-264.
- Lakshmipathy, S., Reyes, D.A., Girmajji, S., 2011. Partially averaged Navier–Stokes method: modeling and simulation of low Reynolds number effects in flow past a circular cylinder. In: 6th AIAA Theoretical Fluid Mechanics Conference, Honolulu, Hawaii. AIAA-2011-3107.
- Ma, J., Peng, S.-H., Davidson, L., Wang, F., 2011. A low Reynolds number variant of partially-averaged Navier–Stokes model for turbulence. *Int. J. Heat Fluid Flow* 32, 652–669.
- Menter, F., Egorov, Y., 2010. The scale adaptive simulation method for unsteady turbulent flow predictions. Part 1: Theory and description. *Flow Turb. Combust.* 85, 113–138.
- Piomelli, U., Balaras, E., Pasinato, H., Squire, K., Spalart, P., 2003. The inner-outer layer interface in large-eddy simulations with wall-layer models. *Int. J. Heat Fluid Flow* 24, 538–550.
- Saric, S., Jakirlic, S., Djugum, A., Tropea, C., 2006. Computational analysis of locally forced flow over a wall-mounted hump at high-Re number. *Int. J. Heat Fluid Flow* 27, 707–720.
- Schiestel, R., Dejoan, A., 2005. Towards a new partially integrated transport model for coarse grid and unsteady turbulent flow simulations. *Theor. Comput. Fluid Dyn.* 18, 443–468.
- Schwaborn, D., 2012. The ATAAC Project. Final Technical Report. Deliverable D1.1-39a of the 7th Framework Project ATAAC, Contract No. ACP8-GA-2009-233710-ATAAC. <<http://cfd.mace.manchester.ac.uk/ATAAC/>>.
- Shur, M.L., Spalart, P., Strelets, M.K., Travin, A., 2008. A hybrid RANS–LES approach with delayed-DES and wall-modelled LES capabilities. *Int. J. Heat Fluid Flow* 29, 1638–1649.
- Spalart, P., 2000. Strategies for turbulence modelling and simulations. *Int. J. Heat Fluid Flow* 21, 252–263.
- Spalart, P., Jou, W.-H., Strelets, M., Allmaras, S., 1997. Comments on the feasibility of LES for wings and on a hybrid RANS/LES approach. In: Liu, C., Liu, Z. (Eds.), *Advances in LES/DNS*, First Int. conf. on DNS/LES. Louisiana Tech University, Greysden Press.
- Temmerman, L., Hadiabadi, M., Leschziner, M., Hanjalic, K., 2005. A hybrid two-layer URANS–LES approach for large eddy simulation at high Reynolds numbers. *Int. J. Heat Fluid Flow* 26, 173–190.
- Travin, A., Shur, M., Strelets, M., Spalart, P., 2000. Detached-eddy simulations past a circular cylinder. *Flow Turb. Combust.* 63, 293–313.
- van Leer, B., 1974. Towards the ultimate conservative difference scheme. Monotonicity and conservation combined in a second order scheme. *J. Comput. Phys.* 14, 361–370.
- Versteegh, H., Malalasekera, W., 1995. *An Introduction to Computational Fluid Dynamics – The Finite Volume Method*. Longman Scientific & Technical, Harlow, England.
- Yakhot, V., Bailey, S., Smits, A., 2010. Scaling of global properties of turbulence and skin friction in pipe and channel flows. *J. Fluid Mech.* 652, 65–73.